Solution structure of a HNA–RNA hybrid

E Lescrinier [1], R Esnouf [2], J Schraml [3], R Busson [1], HA Heus [4], CW Hilbers [4] and P Herdewijn [1]

Background: Synthetic nucleic acid analogues with a conformationally restricted sugar-phosphate backbone are widely used in antisense strategies for biomedical and biochemical applications. The modified backbone protects the oligonucleotides against degradation within the living cell, which allows them to form stable duplexes with sequences in target mRNAs with the aim of arresting their translation. The biologically most active antisense oligonucleotides also trigger cleavage of the target RNA through activation of endogenous RNase H. Systematic studies of synthetic oligonucleotides have also been conducted to delineate the origin of the chirality of DNA and RNA that are both composed of D-nucleosides.

Results: Hexitol nucleic acids (HNA) are the first example of oligonucleotides with a six-membered carbohydrate moiety that can bind strongly and selectively to complementary RNA oligomers. We present the first high resolution nuclear magnetic resonance structure of a HNA oligomer bound to a complementary RNA strand. The HNA–RNA complex forms an anti-parallel heteroduplex and adopts a helical conformation that belongs to the A-type family. Possibly, due to the rigidity of the rigid chair conformation of the six-membered ring both the HNA and RNA strand in the duplex are well defined. The observed absence of end-fraying effects also indicate a reduced conformational flexibility of the HNA–RNA duplex compared to canonical dsRNA or an RNA–DNA duplex.

Conclusions: The P–P distance across the minor groove, which is close to A-form, and the rigid conformation of the HNA–RNA complex, explain its resistance towards degradation by Rnase H. The A-form character of the HNA–RNA duplex and the reduced flexibility of the HNA strand is possibly responsible for the stereoselectivity of HNA templates in non-enzymatic replication of oligonucleotides, supporting the theory that nucleosides with six-membered rings could have existed at some stage in molecular evolution.

[1]Laboratory of Medicinal Chemistry, Rega Institute for Medical Research, Katholieke Universiteit Leuven, Minderbroedersstraat 10, 3000 Leuven, Belgium
[2]Division of Structural Biology, Wellcome Trust Centre for Human Genetics, Roosevelt Drive, Headington, Oxford OX3 7BN, UK
[3]Institute of Chemical Process Fundamentals, Rozvojova 135, 165 02 Prague 6, Czech Republic
[4]NSR Center for Molecular Structure, Design and Synthesis, University of Nijmegen, Nijmegen, The Netherlands

Correspondence: Piet Herdewijn
E-mail: piet.herdewijn@rega.kuleuven.ac.be

Keywords: Anti-parallel heteroduplex; Antisense; Hexitol nucleic acid; Molecular evolution; Nuclear magnetic resonance; Rnase H

Received: **28 April 2000**
Revisions requested: **9 June 2000**
Revisions received: **5 July 2000**
Accepted: **6 July 2000**

Published: **1 August 2000**

Chemistry & Biology 2000, **7**:719–731

1074-5521/00/$ – see front matter

PII: S1074-5521(00)00017-X

Introduction

Hexitol nucleic acids (HNA) represent an interesting class of molecules, as they are the first example of backbone modified oligonucleotides with a six-membered carbohydrate moiety that hybridize strongly and selectively with complementary DNA and RNA [1–3]. The unique structural properties of HNA make them interesting compounds both for antisense purposes and as model systems in prebiotic world studies [4–6]. Other DNA or RNA analogues with six-membered carbohydrate moieties that have been studied, such as *homo*-DNA [7] and *pyranosyl*-RNA [8], only show self-pairing properties and are incapable of hybridizing with natural nucleic acids.

HNA is composed of 2′,3′-dideoxy-1′,5′-anhydro-D-arabino-hexitol nucleosides with 4′-6′ phosphodiester internucleotide linkages and the base (guanine (G), adenine (A), cytosine (C) or thymine (T)) positioned at the 2′-position (Figure 1a). The six-membered ring mimics a furanose ring frozen in a 2′-*exo*,3′-*endo* conformation. It can be seen as an extended furanose, in which a CH_2 group is inserted between the O4′ and C1′ position (Figure 2a,b). The hexitol nucleotides have a conformational preference with the nucleobase in the axial position, as a result from steric restraints caused by the unshared pairs of the hexitol oxygen. Due to this conformational strain the bases stack efficiently, providing limited conformational freedom of the backbone. Circular dichroism (CD) spectra of single stranded HNA and HNA–RNA hybrids are remarkably similar to those of double stranded RNA[2] which led to the presumption that HNA has a preformed A-form like structure which fits very well in the A-form shape of double stranded RNA. Binding and sequence specificity of HNA is conferred by Watson–Crick base pairs [2]. This was demonstrated by the introduction of one or two mismatches into a HNA–RNA duplex, which results in a large destabilization of the complex [2]. Overall, HNA containing duplexes are exceptionally stable compared to natural

duplexes (i.e. dsDNA, dsRNA and RNA–DNA), with the stability decreasing in the order HNA–HNA > HNA–RNA > HNA–DNA [2]. It is the high stability of the HNA–RNA complexes, which suggested the high potential for their use in antisense applications.

The higher stability of the HNA–RNA duplexes is assumed to be a consequence of the tendency of HNA to adopt A-form like structures. This notion was not only based on the aforementioned CD measurements, but also followed from molecular dynamic simulations that predicted the formation of A-type helices for HNA–DNA as well as HNA–RNA duplexes [9]. The presumed A-form character of HNA also became apparent in molecular evolution studies where it was shown to exclusively direct non-enzymatic synthesis of RNA oligonucleotides.

So far no real structural data is available to confirm the presumed A-form character. Here we describe the first high resolution structure of a HNA oligomer bound to a complementary RNA oligomer as determined by nuclear magnetic resonance (NMR). The derived structures show an anti-parallel HNA–RNA duplex hybridized via Watson–Crick base pairs and a helix form that belongs to the A-type family. Torsion angles and helical parameters deviate only marginally from those of typical double stranded RNA. However, minor groove dimensions are different from the A-form, which is discussed in relation to its resistance to RNase H. The A-form character of the HNA–RNA duplex explains the ability of HNA to efficiently catalyze non-enzymatic synthesis of oligonucleotides. Although the occurrence of HNA in a prebiotic world is unlikely, these studies support the suggestion that conformational rigid oligomers could have existed as intermediates in prebiotic evolution.

Results

The atom numbering, chemical structure and torsion angle definition of the HNA used in this work are depicted in Figure 1. Individual residues are composed of a six-membered anhydrohexitol ring that is substituted at the C2′-position by one of the four different nucleobases: A, G, T or C. Adjacent residues are connected by a 4′(*n*) to 6′(*n*+1) phosphodiester linkage. Torsion angles defined in Figure 1b follow the standard notation of natural RNA [10]. Figure 1c shows the duplex sequence studied by NMR. The

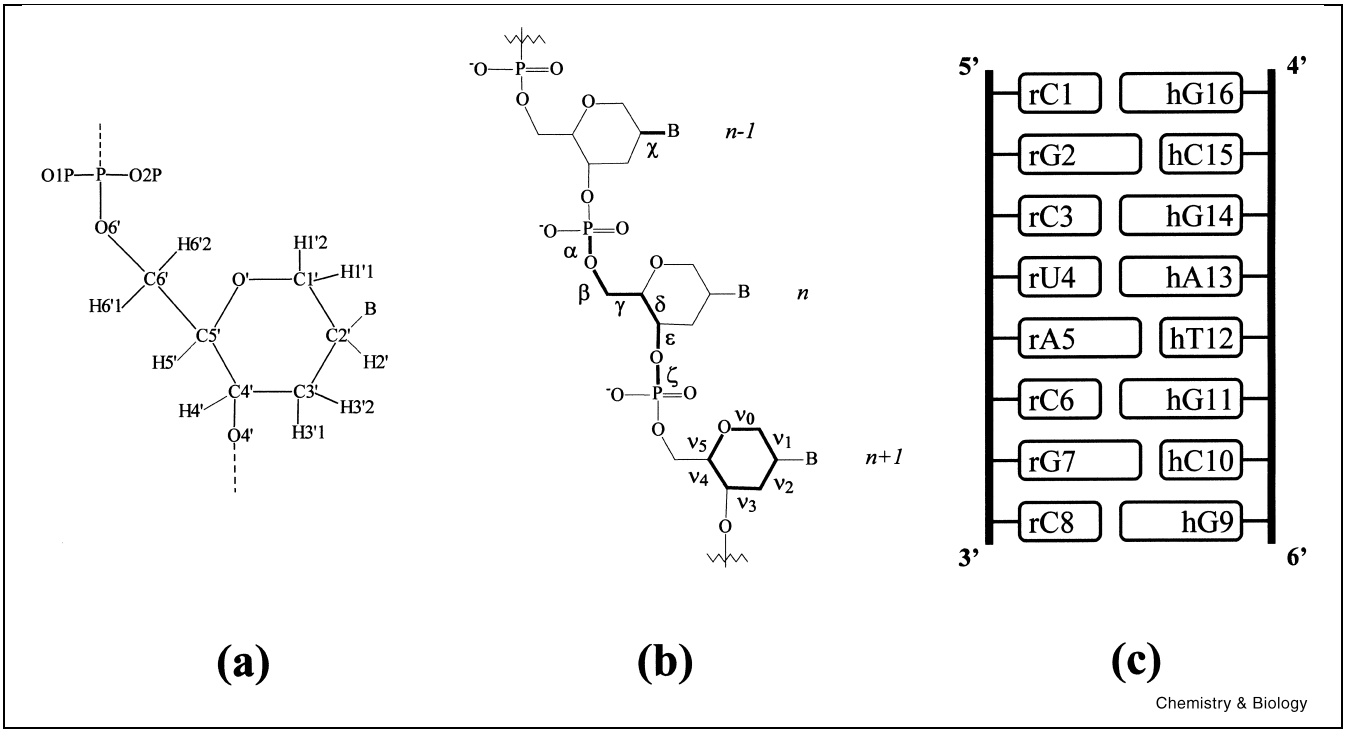

Figure 1. Atom numbering **(a)**, and chemical structure **(b)**, in HNA oligonucleotides used in this manuscript. The main torsion angles that describe the nucleic acid backbone structure are defined as α, β, γ, δ, ε and ζ. The torsion angle χ describes the orientation of the base relative to the sugar. Endocyclic torsion angles of the hexitol ring are defined as ν_0 to ν_5. The base (B) can be adenine, guanine, thymine or cytosine. **(c)** Schematic drawing of the HNA–RNA duplex described in this manuscript. The lowercase letters denote the residue type (r = ribose, h = anhydrohexitol). The numbering of the duplex starts at the 5′-end of the RNA strand and ends at the 4′-end of the HNA strand. A PDI17 residue was attached by a phosphodiester linkage at the 4′-end of the HNA strand during the oligonucleotide synthesis.

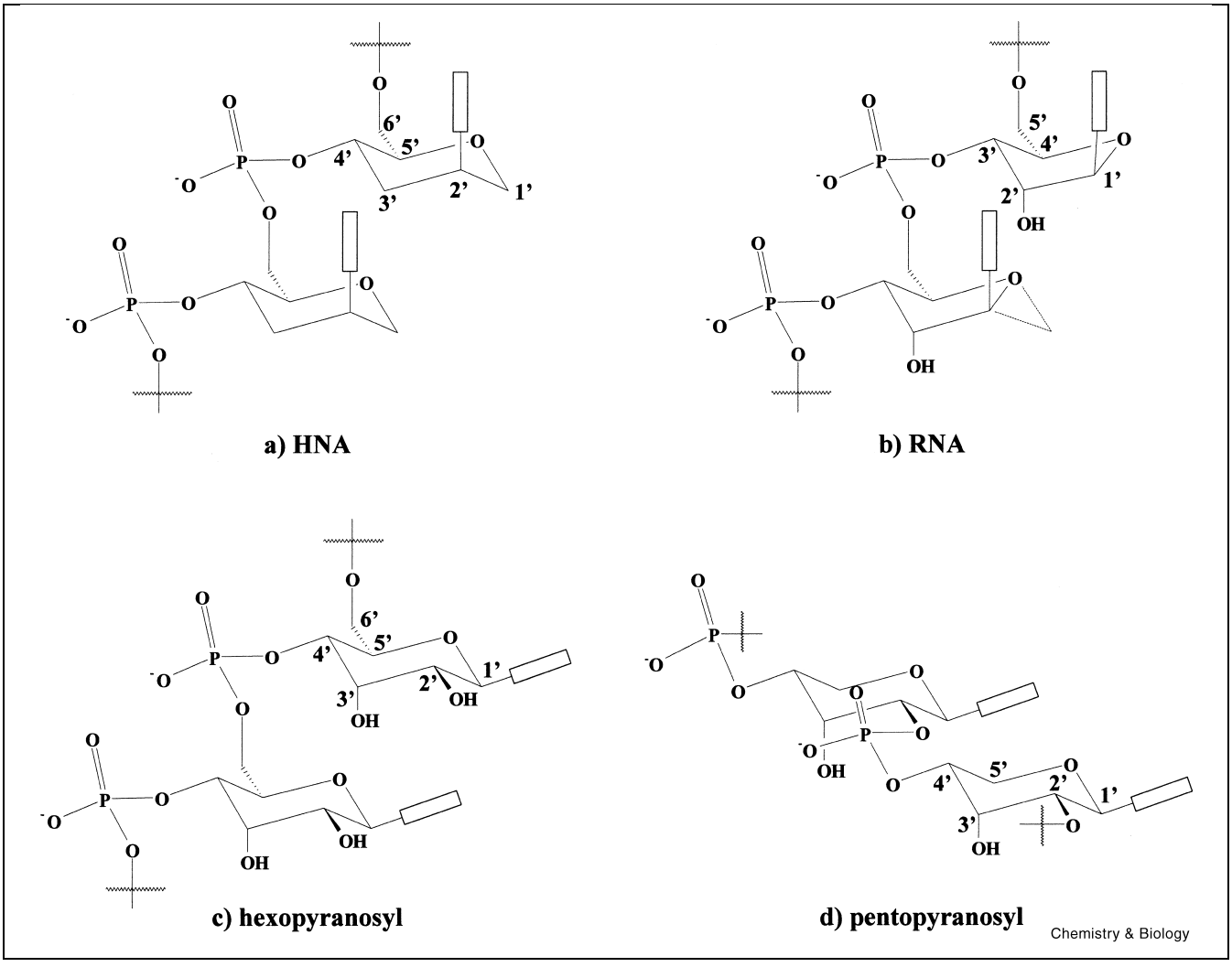

Figure 2. Schematic conformations of various oligonucleotides. **(a)**, HNA (1′-3′-dideoxy (4′→6′) oligonucleotides), **(b)** RNA (ribose (5′→3′ oligonucleotides)), **(c)** hexopyranosyl (4′→6′) oligonucleotide and **(d)** pentopyranosyl (2′→4′) oligonucleotides. The resemblance between the hexitol ring and the ribose can be seen by inserting a CH_2 group between the O4′ and C1′ of the ribose. This is indicated by the dashed line in the schematic RNA structure **(b)**. Homo DNA is a chemical analogue of **(c)**, i.e. containing 2′-3′-dideoxy hexopyranosyl (4′-6′) nucleotides.

selected HNA sequence (6′-GCGTAGCG-4′) is identical to the sequence previously used in the molecular dynamics studies and contains all four nucleobases. The HNA–RNA duplex, used for the NMR experiments, was obtained by titrating an RNA solution (5′-CGCUACGC-3′) with the complementary HNA sequence. One-dimensional (1D) NMR spectra of non-exchangeable base and anomeric protons, monitoring the degree of complex formation during the titration are shown in Figure 3.

The concentration of RNA oligonucleotides was determined using nearest neighbor optical density values taken from the literature [11]. The HNA concentration could only be roughly estimated since there are no reference values available for these modified nucleotides. Initially the amount of HNA was underestimated, resulting in an overshooting during the titration. However, this could easily be corrected by adding more RNA to the mixture (Figure 3, upper trace). This figure also shows the excellent spectral resolution of the HNA–RNA duplex at a 1:1 ratio. The 1:1 complex was used for further investigations.

Assignment of resonances

Non-exchangeable protons in the RNA strand were assigned starting from a standard anomeric to aromatic proton walk [12]. In this way sequential connectivities for the entire RNA strand could be identified, thereby assigning

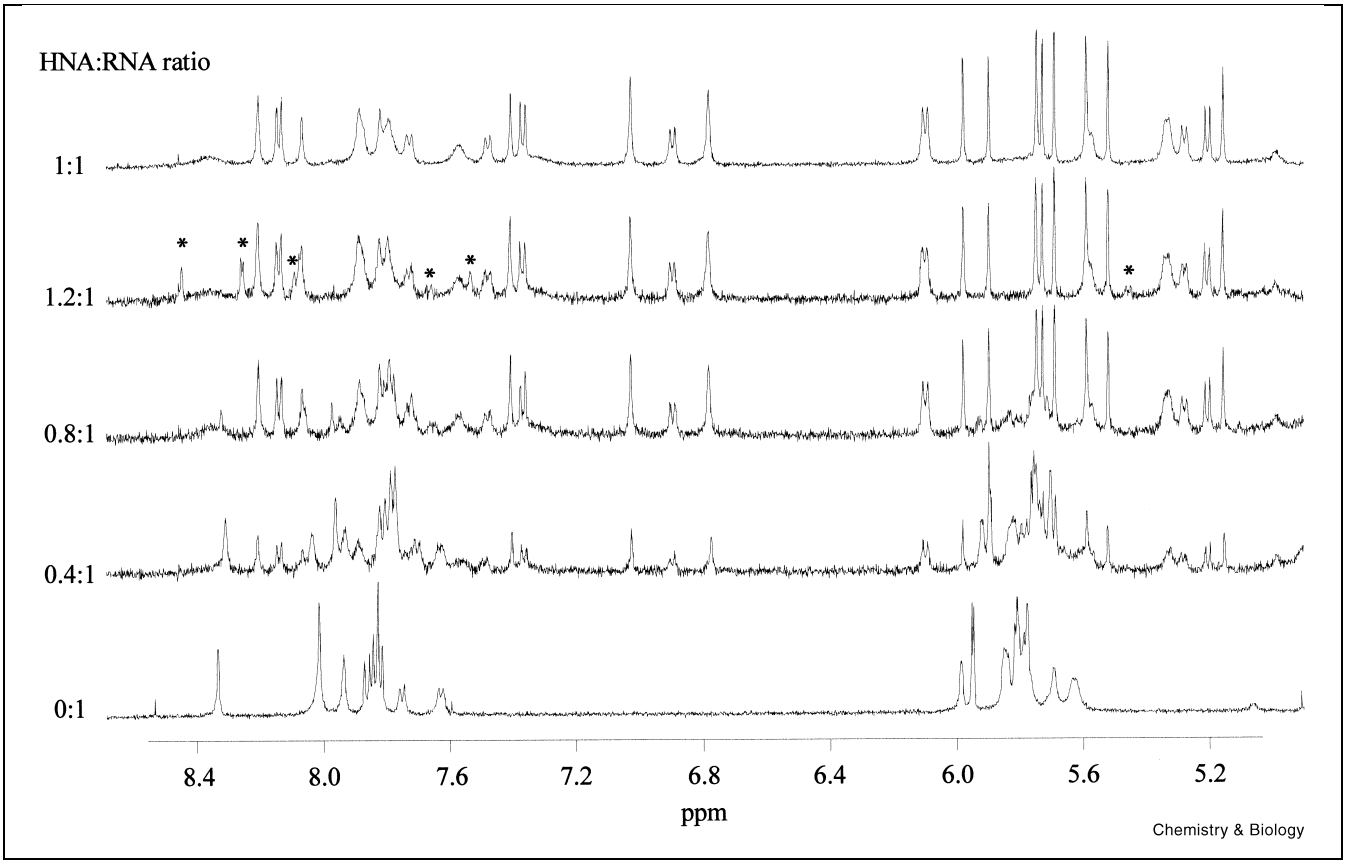

Figure 3. 1D NMR spectra recorded at different steps of the titration of r(CGCUACGC) with h(GCGTAGCG). A solution of 0.874 mmol RNA (pD 7.0) in 0.400 ml D_2O was used as a starting point (spectrum at bottom). * indicates signals originating from excess HNA.

all H1′ and H8/H6 resonances (results not shown). Most of the other sugar resonances of the RNA strand were initially identified by their NOEs [13] to the well-dispersed anomeric and aromatic proton signals. Many of these were confirmed by the strong H3′–H4′ and H5′–H5′ crosspeaks observed for all residues in the TOCSY and DQF-COSY spectra. The 5′- and 3′-terminal residues of the RNA strand showed observable H1′–H2′ TOCSY crosspeaks.

Standard NMR sequential assignment by starting with an aromatic to anomeric proton walk could not be applied to the HNA strand. However, since the C3′ in the HNA strand is not bonded to an oxygen or nitrogen hetero atom, the H3′1 and H3′2 resonate in the high field region between 2.5 and 1.5 ppm, well separated from the rest of the spectrum. These chemical shifts, which are comparable with H2′/2″ chemical shifts of DNA molecules, were used as starting points in the assignment strategy. From the hexitol structure (Figure 4b) it is expected that the H2′ is coupled to both H1′1/H1′2 and H3′1/H3′2, while H4′ is only coupled to H5′ and H3′1/H3′2 in a COSY spectrum. Thus, H2′ resonances could be identified by observing weak (∼2 Hz) tandem crosspeaks in the COSY spectrum to the mutually coupled H3′1/H3′2 and H2′1/H2′2 resonances. H4′ resonances were assigned by observing a single crosspeak to either the H3′1 or H3′2 resonance (∼10 Hz), which were not stereospecifically assigned at this point, as well as by a single crosspeak to H5′ resonance (∼11 Hz). Subsequently H3′1 resonances were stereospecifically assigned by the strong H4′–H3′1 COSY crosspeaks, and H3′2 resonances were assigned from H2′–H3′1/H3′2 TOCSY crosspeaks. The H1′1/1′2 signals were assigned via TOCSY or COSY crosspeaks from H2′. Stereospecific assignment of H1′1 was inferred from strong H1′1–H3′1 connectivities in the 100 ms NOESY spectrum (Figure 4a,b). Strong crosspeaks were also observed from H3′1 to H5′ in the same NOESY spectrum. Only a few of the H6′1/H6′2 crosspeaks resonating in the region between 3.8 and 4.3 ppm could be resolved. Sequential resonance assignments (Figure 4c,d) could be obtained from the intraresidual NOEs between aromatic H8/H6(*n*) to H4′(*n*) and from sequential connectivities between H3′2(*n-1*) and H8/H6(*n*) in the 50 ms NOESY spectrum. Relatively weak sequential crosspeaks, caused by broadening of hA13:H8, hG14:H8 and hC15:H6, were observed between these protons and H3′2. This also applies to

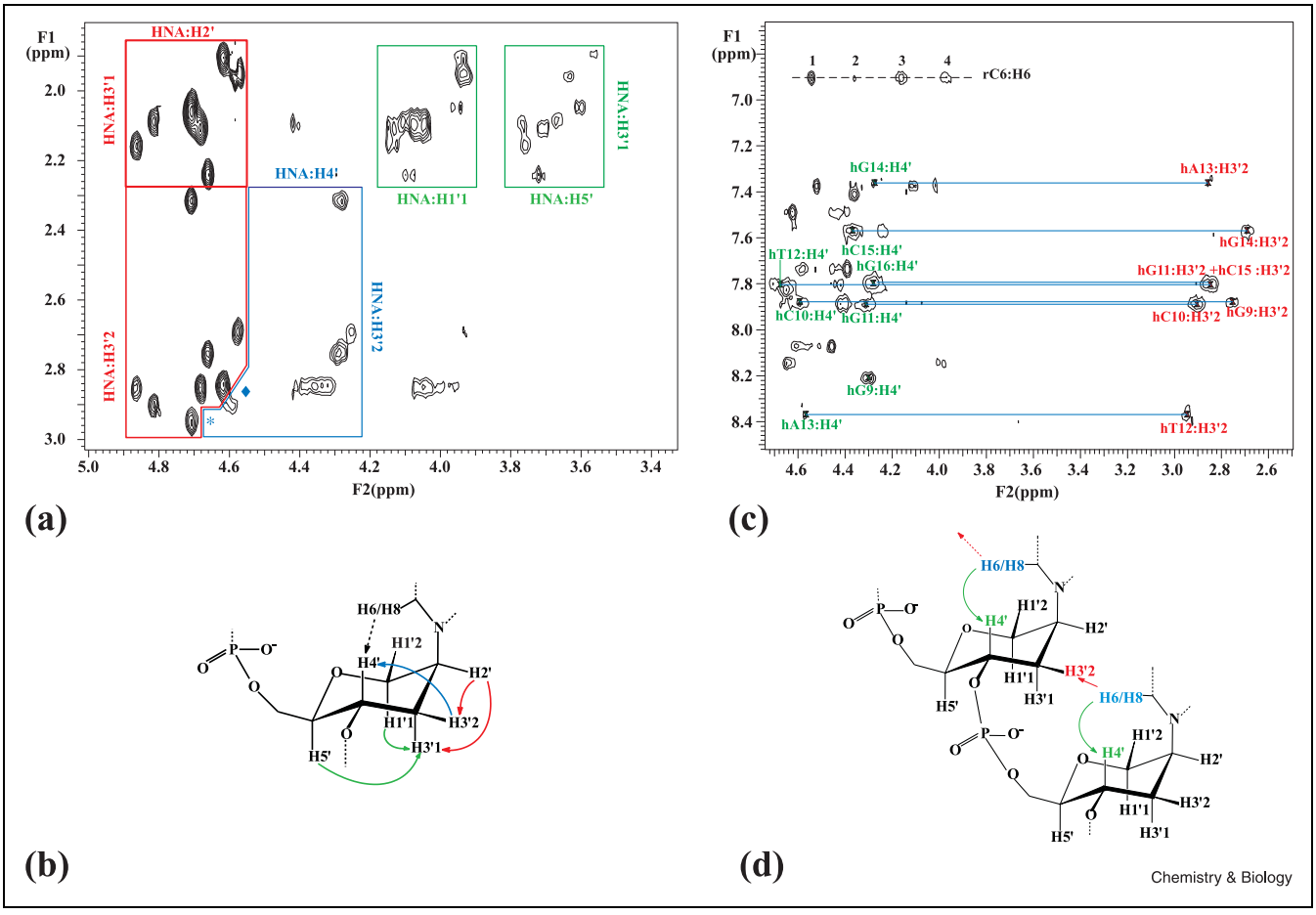

Figure 4. (a) Part of the NOESY spectrum recorded in D_2O (150 ms mixing time, 20°C) showing intra-residue NOE contacts involving hexitol protons. **(b)** Schematic conformation of the hexitol ring conformation, showing distances corresponding to crosspeaks in **(a)**. Missing crosspeaks for residues hT12 and hA13 are indicated by * and ♦, respectively. **(c)** Part of the 2D NOESY spectrum recorded in D_2O (50 ms mixing time, 20°C) showing the sequential resonance assignment of the HNA strand. The sequential crosspeaks between H6/H8 and H3′2 are indicated in red, intra-residue crosspeaks between H6/H8 and H4′ are colored green. The dashed line indicates the unusual upfield shifted rC6:H6 signal with crosspeaks to rA5:H2′ (1), rC6:H2′ (2), rC6:H3′ (3) and rC6:H5″ (4). **(d)** Schematic structure of a HNA dinucleotide showing distances corresponding to crosspeaks marked in the NOESY spectrum in **(c)**.

the connectivities between these protons and H4′. Sequential H4′–P–H6′1/6′2 contacts observed in the 2D [^{1}H, ^{31}P] correlation spectrum (HETCOR) confirmed assignments of these resonances (results not shown).

The existence of Watson–Crick base pairs in an anti-parallel duplex was deduced from 1D imino proton and 2D NOE spectra recorded at 5°C in 90% H_2O/10% D_2O (results not shown). The 1D imino proton spectra showed six sharp and two broad signals between 12.5 and 13.5 ppm. The six sharp signals could be assigned to G–C base pairs via the crosspeaks between imino protons and the H1′ resonances or to A–U/T base pairs via the crosspeaks between the imino and adenine H2 resonances in the 2D watergate-NOESY. These were confirmed by an imino to imino proton sequential walk. The two broad signals for which no crosspeaks were observed in the 2D NOESY, resonate in a region typical for GC base paired imino protons and probably belong to hG1:H1 and hG8:H1.

Derivation of structural restraints

The small $J_{1'-2'}$ couplings, deduced from the absence of H1′–H2′ crosspeaks in the DQF-COSY and TOCSY spectra, combined with the large $J_{3'-4'}$ (~9 Hz) couplings [14] are characteristic of N-type sugars and were observed for all residues in the RNA strand.

The conformation of the HNA six-membered rings can in principle be described by ring puckering parameters, which can be derived from vicinal proton–proton couplings [15,16]. Unfortunately, due to overlap in the DQF-COSY spectrum, the number of coupling constants was not suffi-

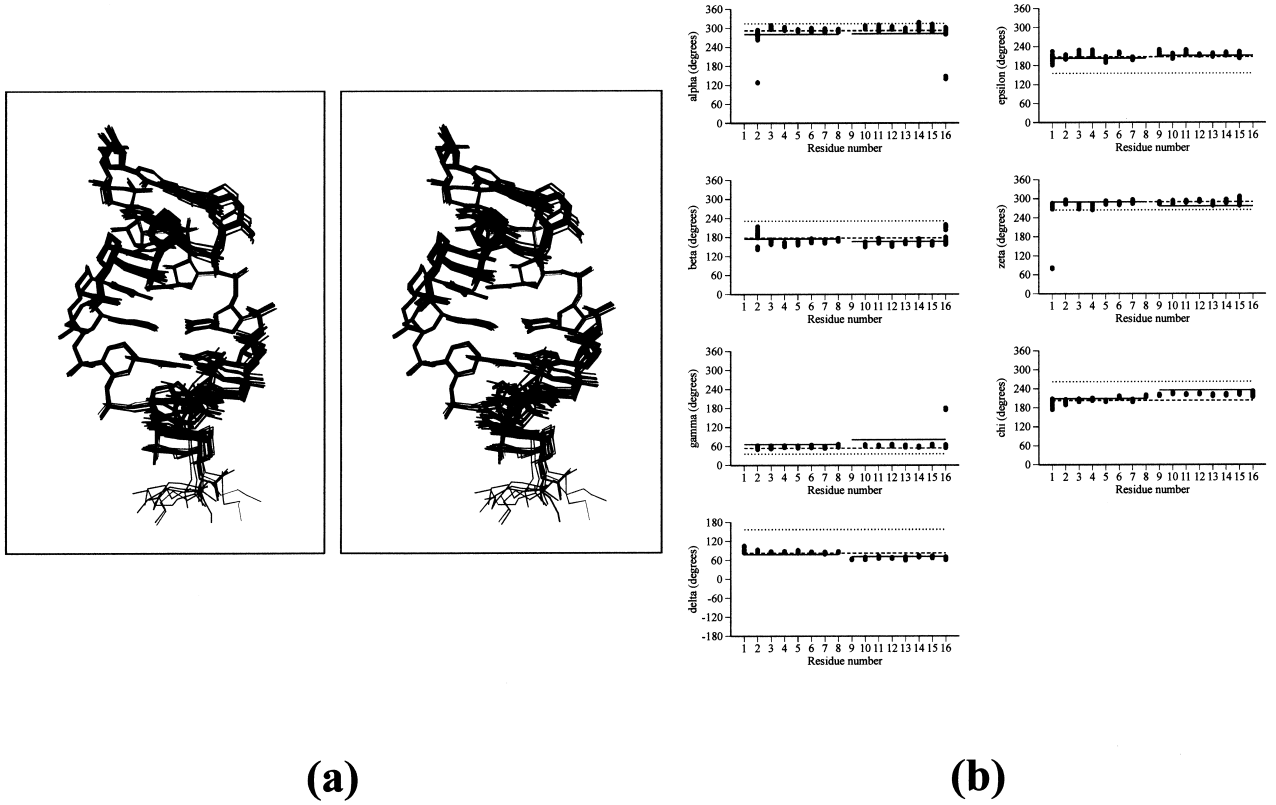

Figure 5. (a) Overlay of the ten structures closest to the average of the final set of 25 structures. Superposition was performed on residues 2–15. **(b)** Variation of the torsion angles for the individual residues of the 25 final structures. For comparison A- and B-form values are given by dashed and dotted lines, respectively. The solid line indicates the average value in the structure obtained previously by molecular modeling [9].

cient to perform a complete conformational analysis. However, strong H4′–H3′1 and H4′–H5′ crosspeaks in the DQF-COSY spectra, which are indicative of large active $J_{H4'-H3'1}$ and $J_{H4'-H5'}$ couplings ($\sim$10 and 11 Hz, respectively), are consistent with an axial position of the coupled protons in the anhydrohexitol ring. Also, very weak or non-observable crosspeaks between H2′ and H3′1 and between the H2′ and H3′2 resonances, correspond with an equatorial position of the H2′ in the HNA strand. Furthermore, the strong intra-residue crosspeaks between the base proton (H8/H6) and the H4′ and close contacts between the H1′1, H3′1 and H5′ resonances were visible in the 100 ms NOESY spectrum. The H4′–H8/H6 NOE contacts are also indicative of an anti-conformation ($\chi = -120 \pm 60°$) of the HNA bases. The combination of all these restraints defines a chair conformation for the hexitol ring with the base in an axial position in correspondence with the previously determined conformation in the monomers [17] and a dimer of HNA [9].

The small passive H4′–H5′/5′ couplings observed in the DQF-COSY H5′–5″ crosspeaks, were used to restrain the

Table 1
Structure statistics for the final set of 25 structures.

Total energy (kcal mol^{-1})	266.2 ± 7.0
NOE violations (> 0.5 Å)	0
Dihedral violations (> 5°)	1 ± 1
RMSD from distance restraints (Å)	0.027 ± 0.002
RMSD from dihedral restraints (°)	0.302 ± 0.467
RMSD from average structure for all heavy atoms (Å)	0.80

RNA γ angles (60 ± 35°). The absence of P–H5′/H5″ cross-peaks in the ^{1}H–^{31}P HETCOR spectrum, indicative of small $J_{P-H5'}$ and $J_{P-H5''}$ restrained β to *trans* (180 ± 30°). The RNA ε angle was restrained to −130 ± 40° based on the large $J_{PH3'}$ (∼11 Hz) measured in the same spectrum. In HNA the ε angle was restrained to −135 ± 60° to prevent the occurrence of conformations in the *gauche*$^{+}$ region which is stereochemically forbidden for this angle [12]. The ^{31}P chemical shift was only used in a qualitative sense to restrain the RNA α and ζ angles to 0 ± 120°. The HNA γ torsion angles were restrained to 60 ± 35° based on the very small $J_{H5'H6'}$ and $J_{H5'-H6''}$ couplings. No other backbone torsion angle restraints were applied to the HNA strand.

Distance restraints were derived from a series of 2D NOE experiments (see Materials and methods section). This resulted in 28 interresidue (eight in HNA, 18 in RNA and two interstrand) and 93 intra-residue (55 in HNA, 38 in RNA) restraints.

Hydrogen bond restraints were deduced from the spectra in H_2O. Thus, three imino imino proton contacts, four imino-H1′ contacts and two imino-H2 contacts were treated as distance restraints in the structure calculations.

Structure determination

Starting from two extended strands, a set of 100 structures was generated by torsion angle dynamics, largely identical to the protocol proposed for a DNA duplex [18] (see Materials and methods section). Out of these, 25 structures with similar low total energies and restraint violations were selected for further refinement by 'gentle molecular dynamics' (see Materials and methods section). These structure calculations and refinements were done twice: once using all experimental restraints and once using only experimental restraints for the HNA strand combined with RNA and HNA hydrogen bond restraints. Both refinements yielded similar structures, indicating that the overall structures were not biased by the RNA restraints that were very typical for right-handed A-type dsRNA. Figure 5a shows superpositions of the ten structures closest to the average of the 25 structures calculated with all experimental restraints. Because the rC1 residue is poorly defined due to insufficient NOE interactions at the helix end, the rC1–rG16 base pair was ignored in the structure superposition. The 1–3 propanediol (PDI17) residue attached to the 4′ end of the HNA strand by a phosphodiester linkage behaves as an independent moiety and shows no interaction with the rest of the molecule. Structure statistics are listed in Table 1. Backbone torsion angle variations in the 25 structures calculated with all experimental restraints are shown in Figure 5b.

Discussion

Description of the structure

The solution structure determination of this HNA–RNA duplex reveals an anti-parallel duplex with standard Watson–Crick base pairs and a helical geometry very similar to A-form dsRNA. Thus, overall the structure is in line with the structure predictions made earlier based on the CD studies [2] and molecular dynamic simulations [9]. The structures are well defined both in the HNA and RNA strand by the high number of NOEs provided by the hexitol rings and the nearly complete torsion angle determination, which is reflected in the small variation in the torsion angle values of the 25 final structures, selected for this analysis (Figure 5b). The narrow conformational space sampled in the MD procedure, which leads to a well-defined overall structure may be a consequence of the rigid chair conformations of the hexitol rings. An example of this is given by the restrained terminal sugar moieties of the RNA strand, which are of the N-type. This fixed sugar pucker conformation contrasts sharply to the behavior typically observed for terminal residues in canonical A and B form helices, which normally display fraying and consequently display mixed N/S-type sugar populations. All backbone torsion angles of the RNA strand are very close to A-form values [19]. Sugar puckers of all RNA residues are in the *2′-exo* to *3′-endo* range (N-type). Also the backbone torsion angles of the HNA strand are close to A-form, although specific but small differences are seen between the two strands: ignoring a few α to ζ or α to γ crankshaft motions for the terminal rC1 and hG16 residues, on average α, γ, ε and ζ are slightly (4–10°) larger, while β is slightly smaller in the HNA strand. The δ and χ torsion angles show somewhat larger differences, i.e. δ is 20° smaller in the HNA strand, while the χ angle is 20° larger. Despite these specific differences the average torsion angles in HNA are very close to the values for A-RNA double helices. Helical parameters of the duplex also show tendencies as in dsRNA A-type helices with a typical small axial rise (3.0 Å), a negative base displacement (−3.5 Å) and an intermediate twist angle of 32–36° per base pair step (first base pair step excluded), along the helical axes (Table 2).

Comparison with the modeled structure

An overall similarity exists between the final NMR structure and the structure obtained by molecular modeling [9]. The average values of β, δ, ε and ζ in the HNA strand and α, β, γ, δ and ζ in the RNA strand are very similar to the average backbone torsion angles in the modeled structure. However, the NMR structure has slightly different α and γ average values in the HNA strand. Compared to the modeled structure, they are both closer to the energetically favorable *gauche*$^{-}$ and *gauche*$^{+}$ conformation, respectively. No dihedral restraints on the α torsion angles were used during the calculation of the NMR structure.

The sugar puckering in both models is very similar. All ribofuranoses adopt an N-type conformation (average phase angle: 7.5 ± 11.3°, average sugar amplitude:

Table 2
Average values of the helical parameters for the final set of 25 HNA–RNA structures with standard deviations in parentheses, the rC1–hG16 base pair was excluded in the calculation of average values and standard deviations for the HNA–RNA duplex.

	X-Displacement (Å)	Rise (Å)	Twist (°)	Tilt angle (°)	Minor groove width (Å)
A-RNA	−5.3	2.9	31.4	positive	11.0
B-DNA	0	3.2	40.5	negative	5.7
HNA–RNA	−3.4 (0.2)	3.0 (0.3)	34.4 (2.3)	1.5 (3.0)	10.0 (0.1)
rC1–hG16	−3.2 (0.3)	3.2 (0.5)	41.1 (10.8)	−7.8 (6.3)	
rG2–hC15	−3.6 (0.3)	3.0 (0.2)	32.3 (1.1)	3.3 (1.4)	10.3 (0.2)
rC3–hG14	−3.4 (0.3)	3.2 (0.2)	34.5 (1.6)	1.7 (1.3)	9.9 (0.1)
rU4–hA13	−3.2 (0.2)	3.1 (0.3)	36.6 (3.1)	−2.4 (1.2)	9.8 (0.1)
rA5–hT12	−3.4 (0.2)	3.0 (0.1)	34.4 (1.0)	4.5 (1.5)	9.9 (0.1)
rC6–hG11	−3.5 (0.2)	3.1 (0.4)	34.1 (2.0)	−1.9 (1.2)	10.1 (0.1)
rG7–hC10	−3.5 (0.2)	2.8 (0.1)	34.2 (2.1)	3.6 (1.2)	
rC8–hG9	−3.5 (0.2)				

36.8 ± 3.8°). The anhydrohexitol rings are in a chair conformation with the base in an axial position.

In the model structure the hexitol ring in hG9 at the HNA 6′-end is flipped into an inverted chair conformation with guanine in an equatorial position [9]. However, our NMR data from the COSY and NOESY spectra indicate that all hexitol rings, including hG9, are in a chair-like conformation with the nucleobases in an axial position.

RNase H specificity

Optimal usage of DNA oligomers in antisense strategies for biomedical treatment and biochemical applications can be achieved when the target RNA–DNA double helix is cleaved by RNase H. The high stability of HNA oligonucleotides and their preference for binding to RNA suggested that HNA would be an excellent DNA analogue for antisense approaches. However, soon after its discovery it was found that HNA–RNA hybrids are a very bad substrate for RNase H [2]. Our NMR derived HNA–DNA structure gives possible explanations for its resistance towards this enzyme. Previously, the elucidation of several RNA–DNA complexes by NMR led to the hypothesis that the minor groove width is a major determinant for RNase H specificity. Specifically, it has been proposed that in order for the RNA–DNA complex to be a suitable substrate for RNase H the minor groove has to be narrowed from ∼11 Å as in canonical dsRNA to about 8–9 Å in RNA–DNA duplexes [20]. In subsequent studies the elucidation of several structures of DNA–RNA hybrids provided further support for this hypothesis [21–23]. Recently this hypothesis has been questioned by Wüthrich et al. [24], who reported an extremely narrow minor groove width of 4.5 Å for an RNA–DNA hybrid involved in reverse transcription of the HIV genome. An alternative hypothesis was put forward by these authors, namely that the conformational flexibility of the deoxyriboses versus riboses would be the key determinant for recognition. Adaptation of the hybrid duplex by changing the sugar puckers of the DNA strand would then enable the RNA–DNA hybrid to be recognized by RNase H in an induced fit mechanism. This induced fit mechanism might also explain the en-

Table 3
Calculated minor groove widths in selected duplexes.

	Minor groove distance (Å)		
	P–P[a]	O4′–O4′[b]	reported
A-helix	11	6	
B-helix	6	4	
r(caugugac): d(GTCACATG)[20]	8.5–8.9	4.9–5.2	8.6–9.0
r(gcca)-d(CTGC): d(GCAGTGGC)[21]	7.8–8.2	4.4–5.4	7.3–7.8
r(gaggacug): d(CAGTCCTC)[22]	8.1–9.7	4.9–5.9	8–9
r(ccugacgc): d(GCGTCAGG)[23]	8.2–9.9	5–5.2	8–10
r(gcaguggc): (gcca)-d(CTGC)[24]	7.2–8.1	3.7–4.8	4.5
r(cgcuacgc): h(GCGTAGCG)	10	4.4–4.8[c]	

RNA residues are in lower case, DNA and HNA residues in upper case.
[a]Minor groove distance was calculated by taking the $P3'_n$–$P3'_{n'+1}$ distance, subtracted by 5.8 Å to account for van der Waals radii of the phosphate groups.
[b]Likewise by taking the $O4'_n$–$O4'_{n'+2}$ distance subtracted by 2.8 Å.
[c]Likewise by taking the $hC1'_n$–$O4'_{n'+2}$ distance subtracted by 3.1 Å.

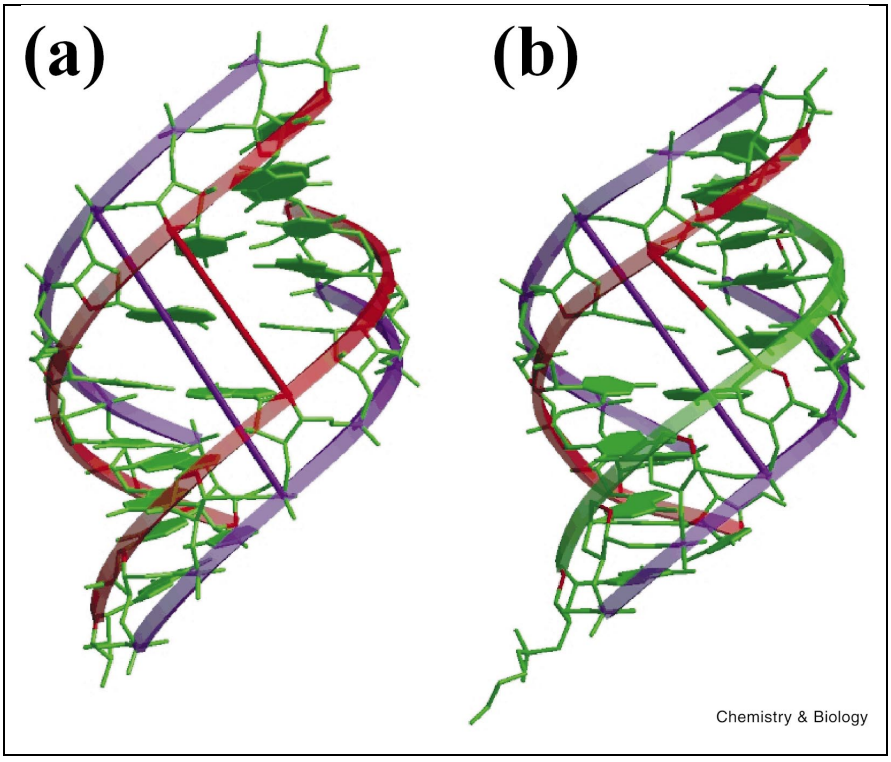

Figure 6. (a) View into the minor groove of an A-form dsRNA helix. Distances used in the determination of minor groove widths, i.e. P3′$_n$–P3′$_{n'+1}$ and O4′$_n$–O4′$_{n'+2}$ are indicated for two examples by magenta and red tubes, respectively. **(b)** A similar view into the minor groove of the HNA–RNA structure closest to the average, showing corresponding P3′$_n$–P3′$_{n'+1}$ and hC1′$_n$–O4′$_{n'+2}$ distances. Ribbons through phosphorous atoms are colored in magenta, those through O4′ in the RNA strands in red and those through C1′ in the HNA strand in green. (Figure was generated using Bobscript2.4 [40], a modified version of Molscript1.4 [41] and rendered with Raster3D [42].)

hanced dNTPs incorporation by HIV reverse transcriptase after the enzyme has passed the tRNA–RNA primer template duplex.

Part of the controversy concerning the minor groove hypothesis lies in the different definitions used by different groups to calculate groove widths, which has led to confusion and unnecessary misunderstandings. Two definitions prevail to calculate the minor groove width (Figure 6a): (1) perpendicular separation of helix strands drawn through phosphate groups, diminished by 5.8 Å to account for the van der Waals radii of the phosphate groups, or (2) analogously, through O4′ groups, diminished by 2.8 Å. Table 3 gives an overview of minor groove widths of published structures using these two definitions. A comparison of the minor groove distances reveals a narrowed minor groove for all RNA–DNA hybrids that are a substrate for RNase H, with all duplexes containing stretches in the range of 8–9 Å, which is in line with the original proposal of Reid et al. [20]. In this respect the hybrid molecule studied by Wüthrich et al. [24] does not behave differently. The extremely narrow minor groove width reported by these authors is simply a consequence of using O4′–O4′ distances rather than P–P distances. Including the HNA–RNA duplex in this discussion is more complex, since it can easily be seen from the view into the minor groove (Figure 6b) that neither the P–P nor the O4′–O4′ distances are a good measure of the groove width since neither of these determine the outer shell of the minor groove. Instead the outer shell of the HNA–RNA duplex is given by the hC1′–rO4′ distance, which corresponds to a minor groove width of 4.4–4.8 Å, comparable to the widths calculated from the O4′–O4′ distances in the other duplexes. However, the minor groove width calculated from the P–P distances comes close to that in A-form dsRNA, which might be the reason for its resistance towards RNase H. Thus, it seems likely that not the minor groove width per se, but rather the P–P distance across the minor groove is a major determinant for RNase H specificity. This would agree with the enzyme making specific contacts to both the scissible phosphate diester bond in the RNA strand and to opposite DNA phosphates, as was proposed from the early model docking studies [20]. Alternatively or additionally, adaptability of the DNA strand in an induced fit mechanism as proposed by Wüthrich et al. might be important. Because the HNA strand in the HNA–RNA duplex is very rigid the hexitol rings are not apt to conformational flexibility, which hinders induced fitting of the duplex upon binding to RNase H.

Possible implications for molecular evolution in a prebiotic world

For our understanding of molecular evolution in a prebiotic world, delineating the stereochemical grounds that could have evolved nucleic acids with riboses or deoxyriboses in present day biochemistry would constitute a major im-

provement. To achieve this goal Eschenmoser et al. have systematically studied stereochemical aspects of various RNA and DNA analogues, which have in common that the RNA derivatives are aldosugars with multiples of CH_2O groups [25,26] from which the DNA analogues are derivatized by deoxylation at specific sites [8]. One of the key questions in these studies is why five-membered furanose rings, i.e. ribose and deoxyriboses were selected during evolution, while the six-membered pyranose rings were discriminated against. From all nucleic acid derivatives studied to date HNA is the only sugar modified analogue with a six-membered ring that is capable of binding to natural occurring nucleic acids, rather than showing mere self-pairing, i.e. the suite of hexopyranosyl (4′–6′) oligonucleotides and pentopyranosyl (2′–4′) oligonucleotides studied by Eschenmoser et al. were all incapable of binding to RNA, but can form very stable self-complementary duplexes. In the case of the pentopyranosyl family, self-complementary duplexes of all four members were much stronger than duplex RNA, which led to the conclusion that stability per se was not a criterion for selection. The high resolution structure of a member of the hexopyranose family, i.e. 2′,3′-dideoxyglucopyranosyl (6′–4′) oligonucleotides termed *homo*-DNA, showed Watson–Crick base pairing with the strands in an anti-parallel orientation [7]. However, a major structural difference was revealed, in that the structure contains an average base pair distance of 4.5 Å leading to a quasi-linear structure rather than a helical one. Although there is no high resolution structure available for the pentopyranosyl family the observed cross-pairing between all members and preliminary NMR data suggests a common quasilinear structure with a similar large helical rise for this compound [26]. HNA on the other hand shows a normal helical rise of $\sim$3 Å, which matches the position of the bases in canonical dsRNA. This is probably the major reason why HNA is capable of binding RNA, while the others are not. The chemical difference between HNA and the other two families can be pinpointed to where the base and phosphodiester group are attached to the sugar moiety (Figure 2). In the case of the pentopyranosyl family, the backbone enters and leaves the sugar at its 4′ and 2′ positions, respectively, while for the hexopyranosyl family and HNA molecules corresponding entry and exit sites are 5′ and 4′. Also the bases in HNA and RNA are in an axial position, while those of the pentose and hexose families are in an equatorial position. In other words, relative to the pentopyranose family the backbone of HNA is shifted two positions, while relative to hexopyranose the base is shifted one position from 2′ to 1′. These changes make the bases in the pento- and hexopyranosyl nucleic acids more distant from the sugar-phosphate backbone than in HNA or RNA. Apparently these changes do not permit binding to natural nucleic acids, because these duplexes are driven into an extended quasi-linear conformation that does not match canonical dsRNA or dsDNA structures. On the other hand, although HNA also contains a six-membered ring, it's relative position to the sugar-phosphate backbone and the position of the base allows it to bind to RNA. This gives further support that, although not experimentally proven, six-membered rings could have existed as an intermediate in molecular evolution, but somehow became extinct. Despite the structural similarity between HNA and RNA as well as its binding preference for RNA also this structural mimic was not chosen to survive during evolution, possibly because of its difficult synthesis under prebiotic conditions and its rigid structure. The rigid six-membered hexitol rings do not display similar atomic ring mobilities as five-membered furanose ring systems that interconvert easily between N- and S-type conformations over small energy barriers. Therefore they lack sufficient structural flexibility, HNA for instance only binds weakly to DNA. Therefore, if flexibility was an important criterion for selection the relative rigidity of the six-membered rings might have been a driving force for these types of compounds to become extinct. Finally, we note that, in accordance with Eschenmosers note on pentopyranosyl oligonucleotides, HNA–RNA duplexes are very stable and, hence, that stability probably has not been a selection criterion for the evolution of nucleic acids.

Another important issue related to molecular evolution in a prebiotic world is the selection of D-nucleotides. To assay this chiral selection Joyce, Orgel and collaborators have investigated non-enzymatic replication of oligonucleotides on various RNA and DNA templates using activated nucleoside 5′-phosphates [27]. In these studies L-enantiomers added in the reaction mixture serve as a potent inhibitor of the oligomerization. Selection of the L-enantiomer leads to chain termination, and thus the extent of selection can be determined by monitoring the amounts of different lengths of the formed oligomers. Following this approach, recently Orgel et al. [4–6] showed that HNA is a more efficient template for the catalysis of RNA oligonucleotides with greater stereospecificity for D-enantiomers than either RNA or DNA templates. As suggested by Orgel et al. the presumed typical A-form of the HNA–RNA duplex that we now observe in our derived structure could be a reason for its enhancement of non-enzymatic oligonucleotide synthesis. However, the structure observed for the 3′-end of the RNA strand in the HNA–RNA duplex, offers another intriguing possibility. In RNA and DNA duplexes the terminal base pairs show an appreciable fraying effect resulting in mixed populations of N- and S-type sugars. In the HNA–RNA duplex the 3′-terminal residue maintains a pure N-type sugar conformation and the fraying process is virtually arrested. In the chiral selection assays, an L-nucleotide binds to the template through initial formation of a standard Watson–Crick base pair. However, as can be seen from Figure 7, without local adaptation of the sugar-phosphate backbone steric hindrance between the 3′-terminal D-nucleotide and the incoming L-ribose will prevent a di-

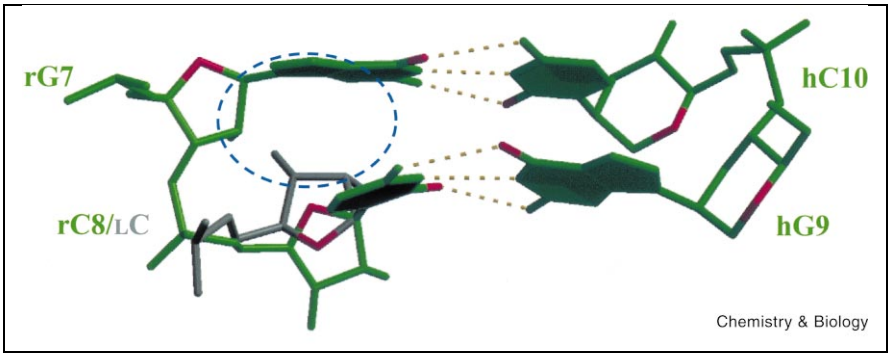

Figure 7. Model of extending a growing RNA chain on a HNA template by an L-nucleotide. This is illustrated by superimposing the base of an incoming L-cytidine on the cytidine base of the 3′-terminal RNA residue in the NMR derived structure of the HNA–RNA heteroduplex. Thus, it can be seen that initial Watson–Crick base pair formation of the L-cytidine base with the HNA template creates steric hindrance between the 3′-terminal nucleotide and the L-ribose. This is caused by the inverted orientation of the L-ribose, which after adaptation of the sugar-phosphate backbone and subsequent incorporation leads to chain termination. The two terminal base pairs of the HNA–RNA structure are in green, the L-cytidine 5′-phosphate (LC) is in grey. The blue ellipse indicates steric hindrance.

rect close approach of the 3′-hydroxyl and 5′-phosphate. Therefore, incorporation of the L-nucleotide at the 3′-end of a growing RNA chain asks for a certain degree of conformational flexibility, which is apparently easier provided by the typical fraying 3′-helix ends of canonical dsRNA or an RNA–DNA duplex. Thus, the rigid A-type HNA–RNA helix renders the HNA template more critical in discriminating against the L-enantiomer and therefore more stereoselective for the D-enantiomer.

Conclusions

The present NMR data are the first accurate experimental evidence of the helical shape of HNA–RNA duplexes and show their similarity with the natural A-form nucleic acid complexes.

It is clear that HNA can adopt a conformation, which is similar to the geometry of dsRNA in an A-form duplex, despite the fact that HNA has a rigid 1,5-anhydrohexitol sugar moiety whereas the RNA backbone is built from phosphorylated ribofuranose units. Possibly, due to the rigidity of the six-membered ring, both the HNA and the RNA strand in the HNA–RNA duplex structure are well defined. The well-defined HNA–RNA structure as well as the minor groove width of the HNA–RNA duplex can explain why HNA–RNA duplexes can bind to RNase H, but is only a weak substrate for degradation by the enzyme.

The A-form character of a nucleic acid with a six-membered ring, which is capable of binding to RNA gives further support to the notion that somewhere during prebiotic molecular evolution nucleic acids with a six-membered ring could have existed but somehow became extinct due to their rigidity, which is incompatible with processes where flexibility is needed.

Significance

The structure of a HNA–RNA duplex is used in this article to explain the properties of antisense constructs, containing HNA oligonucleotides bound to RNA targets. This information can serve in new projects for the design of more efficient synthetic nucleic acids.

Revealing the mechanism of RNase H is an important issue in antisense development, since degradation of the RNA strand in an oligonucleotide–RNA complex is considered as a favorable aspect of antisense oligonucleotides. Our structural results support the notion that the P–P distance across the minor groove is a major determinant for degradation of RNA by RNase H. The flexibility of the DNA strand in DNA–RNA complexes, allowing for induced fit mechanisms in binding RNase H, might be an additional factor for degradation of the RNA strand.

Based on the presented data, a possible role for conformational restricted nucleic acids, such as nucleic acids with a six-membered carbohydrate moiety, is presented. The reduced conformational freedom of the hexitol rings in HNA, which forces them into a rigid A-form helix allows them to stereospecifically select D-enantiomers in non-enzymatic replication of oligonucleotides. Thus, conformational restricted nucleic acids containing six-membered sugar rings could have existed as intermediates in prebiotic molecular evolution that selected an enantiospecific RNA world.

Materials and methods

Sample preparation

The RNA strand r(CGCUACGC) was purchased from Eurogentec. Synthesis of the HNA molecule h(GCGTAGCG) was done using phosphoramidite chemistry as described before [9]. The HNA phosphoramidite building blocks were synthesized as described previously [28].

Oligonucleotide strands were dissolved in D_2O and the pD was adjusted to 7. The RNA solution was titrated with a HNA solution to obtain an equimolar mixture. After adding each aliquot of the HNA solution, the mixture was briefly heated to 80°C and slowly cooled to room temperature to allow for duplex formation. The degree of complex formation was monitored by 1D proton NMR. After reaching the 1:1 RNA:HNA titration point the sample was lyophilized and dissolved in 0.75 ml D_2O yielding a 1.7 mM duplex solution. For recording spectra in H_2O, the sample was lyophilized and dissolved in a 0.75 ml 90% H_2O/10% D_2O mixture.

NMR spectroscopy

NMR spectra were recorded on a Varian 500 unity spectrometer operating at 499.505 MHz. Quadrature detection was achieved by States–Haberkorn hypercomplex mode [29]. Spectra were processed using the FELIX 97.00 software package (Biosym Technologies, San Diego, CA, USA) running on a Silicon Graphics Indigo2 R10000 workstation (IRIX version 6.2).

For samples in H_2O 1D spectra were recorded using a jump-return observation pulse [30]. The 2D NOESY of samples in H_2O was recorded at 5°C with a 150 ms mixing time using the watergate sequence [31], using a sweep width of 11000 Hz in both dimensions. The spectrum was recorded with 64 scans for each FID and 4096 data points in t_2 and 512 FIDs in t_1.

The 2D DQF-COSY [32], TOCSY [33] and NOESY [34] spectra of the sample dissolved in D_2O were recorded with a sweep width of 4200 Hz in both dimensions. The ^{31}P decoupled and coupled ^{31}P DQF-COSY spectra were recorded with 4096 datapoints in t_2 and 360 increments in t_1. For the TOCSY experiment, a Clean MLEV17 [35] version was used, with a low power 90° pulse of 26.6 μs and the delay set to 69.2 μs. The total TOCSY mixing time was set to 65 ms. The spectrum was acquired with 32 scans, 2048 data points in t_2 and 512 FIDs in t_1. The NOESY spectra were recorded with mixing times of 50, 100, 150, 200, 250 and 300 ms. Each experiment was recorded with 64 scans for each FID, 2048 datapoints in t_2 and 512 increments in t_1. The ^1H–^{31}P HETCOR [36] spectrum was recorded on a Varian unity+500 spectrometer operating at 499.930 MHz using 4096 datapoints in the proton dimension (t_2) and 400 real datapoints in the phosphorus dimension (t_1), over sweep widths of 5000 and 3000 Hz, respectively. For each FID, 64 scans were collected. All 2D data were apodized with a shifted sine bell squared function in both dimensions and processed to a 4K × 2K matrix in the case of the NOESY and TOCSY spectra and to a 4K × 1K matrix in the case of the DQF-COSY and HETCOR spectra.

Derivation of distance restraints

Proton–proton distance restraints were derived from buildup curves calculated from NOESY spectra with 50, 100, 150, 200, 250 and 300 ms mixing times using the FELIX97.00 software (Biosym technologies). Upper and lower bounds were set to 20% of the calculated distance. Internal references were H5′–H3′1 and H1′1 to H3′1 NOEs, corresponding to 2.72 and 2.78 Å, respectively, in the anhydrohexitol ring and the cytosine H5 to H6 NOEs, corresponding to 2.45 Å. Nine hydrogen bond distance restraints were inferred from observed imino proton contacts in the 2D watergate NOESY recorded in H_2O.

Structure determination

All structure calculations were performed with X-PLOR V3.518 [37]. The topallhdg.dna and parallhdg.dna were modified to include HNA oligonucleotides. In the topology file, the 6′-phosphorylated HNA monomers were introduced as individual residues that can be patched to each other to form a HNA oligonucleotide, comparable to the treatment of RNA and DNA in the standard XPLOR program. Typical parameters of the hexitol ring were added to the standard parallhdg.dna parameter file.

The torsion angle dynamics protocol used was largely identical to that proposed for a DNA duplex [18]. Starting from two extended strands with random torsion angles a set of 100 structures was generated by torsion angle dynamics. The torsion angle dynamics procedure consisted of four different stages. In the first stage an initial search (60 ps in steps of 0.015 ps) of torsion angle space at high temperature (20 000 K) was performed with a decreased weight on the repulsive energy term ($\omega_{vdw} = 0.1$) to facilitate rotational barrier crossing. The coefficients for the dihedral energy term and the NOE energy term were set to 5 ($\omega_{dihedral}$) and 150 (ω_{NOE}), respectively. During the second stage (90 ps in steps of 0.015 ps), the temperature of the system was gradually cooled down from 20 000 to 1000 K, while the ω_{vdw} parameter was gradually increased to 1.0. The third stage consisted of a slow cooling Cartesian molecular dynamics step of 6 ps (0.003 ps timesteps). A 1000-step conjugate gradient minimization was performed during the last stage with the $\omega_{dihedral}$ parameter set to 400 and the ω_{NOE} parameter set to 50.

After the torsion angle dynamics round, the majority of the structures (77%) converted to virtually the same structure with similar total energies (400–500 kcal mol^{-1}) and comparable violations on the NOE and dihedral restraints (0–3 > 0.5 Å and 0–6 > 5°, respectively). The 25 lowest energy structures with less than four dihedral angle violations, were used for further refinement during the 'gentle molecular dynamics' round. This final refinement started with a constant temperature molecular dynamics at 300 K during 20 ps (20 000 steps of 0.001 ps) and was followed by a 200-step conjugate gradient minimization on the average structure of the last 10 ps in the previous dynamics procedure.

Helix parameters were calculated using Curves 5.0 [38,39], which was modified to handle HNA.

The refined coordinates of the ten structures closest to the average are deposited in the Brookhaven Protein Data Bank (PDB ID 1EJZ) together with the measured chemical shifts and experimental restraints.

References

1. Hendrix, C., Rosemeyer, H., Verheggen, I., Seela, F., Van Aerschot, A. & Herdewijn, P. (1997). 1′,5′-Anhydrohexitol oligonucleotides: synthesis, base pairing and recognition by regular oligodeoxyribonucleotides and oligoribonucleotides. *Chem. Eur. J.* **3**, 110C–120C.
2. Hendrix, C., Rosemeyer, H., De Bouvere, B., Van Aerschot, A., Seela, F. & Herdewijn, P. (1997). 1′,5′-Anhydrohexitol oligonucleotides: hybridisation and strand displacement with oligoribonucleotides, interaction with RNase H and HIV reverse transcriptase. *Chem. Eur. J.* **3**, 1513–1520.
3. Van Aerschot, A., Verheggen, I., Hendrix, C. & Herdewijn, P. (1995). 1,5-Anhydrohexit-Nucleinsauren, neue potentielle Antisense-Wirkstoffe. *Angew. Chem.* **107**, 1483–1485.
4. Kozlov, I.A., Politis, P.K., Pitch, S., Herdewijn, P. & Orgel, L.E. (1999). A highly enantio-selective hexitol nucleic acid template for nonenzymatic oligoguanylate synthesis. *J. Am. Chem. Soc.* **121**, 1108–1109.
5. Kozlov, I.A., Politis, P.K., Van Aerschot, A., Busson, R., Herdewijn, P. & Orgel, L.E. (1999). Nonenzymatic synthesis of RNA and DNA oligomers on hexitol nucleic acid templates: the importance of the a structure. *J. Am. Chem. Soc.* **121**, 2653–2656.
6. Kozlov, I.A., De Bouvere, B., Van Aerschot, A., Herdewijn, P. & Orgel, L.E. (1999). Efficient transfer of information from hexitol nucleic acids to RNA during nonenzymatic oligomerization. *J. Am. Chem. Soc.* **121**, 5856–5859.

[7]. Otting, G., Billeter, M., Wüthrich, K., Roth, H.J., Leuman, C. & Eschenmoser, A. (1993). Warum Pentose- und nicht Hexose-Nucleinsäuren? Teil IV. 'Homo-DNS' 1H-, 13C-, 31P- und 15N-NMR-spektroskopische Untersuchung von ddGlc(A-A-A-A-A-T-T-T-T-T)-in wässriger Lösung. *Helv. Chim. Acta* **76**, 2701–2756.

8. Bolli, M., Micura, R., Pitsch, S. & Eschenmoser, A. (1997). Pyranosyl-RNA: further observations on replication. *Helv. Chim. Acta* **80**, 1901–1951.
9. De Winter, H., Lescrinier, E., Van Aerschot, A. & Herdewijn, P. (1998). Minor groove solvatation contributes to the relative stability

of HNA/RNA hybrids as compared to HNA/DNA complexes. *J. Am. Chem. Soc.* **120**, 5381–5394.
10. IUPAC-IUB Joint Commission on Biochemical Nomenclature (1983). *Eur. J. Biochem.* **131**, 9–15.
11. Puglisi, I.Jr. & Tinoco, J.D. (1989). Absorbance melting curves of RNA. *Methods Enzymol.* **180**, 304–325.
12. Wijmenga, S.S., Mooren, M.W. & Hilbers, C.W. (1993). NMR of nucleic acids; from spectrum to structure. In *NMR of Macromolecules: A Practical Approach.* (Roberts, G., ed.), pp. 217–288, Oxford University Press, Oxford.
13. Varani, G. & Tinoco, I. (1991). RNA structure and NMR spectroscopy. *Q. Rev. Biophys.* **24**, 479–532.
14. van de Ven, F.J. & Hilbers, C.W. (1988). Nucleic acids and nuclear magnetic resonance. *Eur. J. Biochem.* **178**, 1–38.
15. Haasnoot, C.A.G. (1992). The conformation of six-membered rings decribed by puckering coordinates derived from endocyclic torsion angles. *J. Am. Chem. Soc.* **114**, 882–887.
16. Haasnoot, C.A.G. (1993). Conformational analysis of six-membered rings in solution: ring puckering coordinates derived from vicinal NMR proton–proton coupling constants. *J. Am. Chem. Soc.* **115**, 1460–1468.
17. Verheggen, I., Van Aerschot, A., Toppet, S., Snoeck, R., Janssen, G., Balzarini, J., De Clercq, E. & Herdewijn, P. (1993). Synthesis and antiherpes virus activity of 1,5-anhydrohexitol nucleosides. *J. Med. Chem.* **36**, 2033–2040.
18. Stein, E.G., Rice, L.M. & Brünger, A.T. (1997). Torsion-angle molecular dynamics as a new efficient tool for NMR structure calculation. *J. Magn. Reson.* **124**, 154–164.
19. Saenger, W. (1984). *Principles of Nucleic Acid Structure*. Springer, New York.
20. Fedoroff, O.Y., Salazar, M. & Reid, B. (1993). Structure of a DNA: RNA hybrid duplex. Why RNase H does not cleave pure RNA. *J. Mol. Biol.* **233**, 509–523.
21. Fedoroff, O.Y., Salazar, M. & Reid, B.R. (1996). Structural variation among retroviral primer-DNA junctions: solution structure of the HIV-1 (−)-strand Okazaki fragment r(gcca)d(CTGC).d(GCAGTGGC). *Biochem.* **35**, 11070–11080.
22. Fedoroff, O.Y., Ge, Y. & Reid, B.R. (1997). Solution structure of r(gaggacug):d(CAGTCCTC) hybrid: implications for the initiation of HIV-1 (+)-strand synthesis. *J. Mol. Biol.* **269**, 225–239.
23. Bachelin, M., Hessler, G., Kurz, G., Hacia, J.G., Dervan, P.B. & Kessler, H. (1998). Structure of a stereoregular phosphorothioate DNA/RNA duplex. *Nat. Struct. Biol.* **5**, 271–276.
24. Syperski, T., Götte, M., Billeter, M., Perola, E., Cellai, L., Heumann, H. & Wüthrich, K. (1999). NMR structure of the chimeric hybrid duplex r(gcaguggc).r(gcca)d(CTGC) comprising the tRNA–DNA junction formed during initiation of HIV-1 reverse transcription. *J. Biomol. NMR* **13**, 343–355.
25. Pitsch, S., Wendeborn, S., Jaun, B. & Eschenmoser, A. (1993). Why pentose- and not hexose-nucleic acids? Part VII. Pyranosyl-RNA (p-RNA) A. *Helv. Chim. Acta* **76**, 2161–2183.
26. Beier, M., Reck, F., Wagner, T., Krishnamurthy, R. & Eschenmoser, A. (1999). Chemical etiology of nucleic acid structure: comparing pentopyranosyl-(2′→4′) oligonucleotides with RNA. *Science* **283**, 699–703.
27. Joyce, G.F., Visser, G.M., van Boeckel, C.A.A., van Boom, J.H., Orgel, L.E. & van Westrenen, J. (1984). Chiral selection in poly-(C)-directed synthesis of oligo(G). *Nature* **310**, 602–604.
28. De Bouvere, B., Kerremans, L., Rozenski, J., Janssen, G., Van Aerschot, A., Claes, P., Busson, R. & Herdewijn, P. (1997). Improved synthesis of anhydrohexitol building blocks for oligonucleotide synthesis. *Liebigs Ann.*, 1453–1461.
29. States, D.J., Haberkorn, R.A. & Ruben, D.J. (1982). A two-dimensional nuclear overhauser experiment with pure absorption phase quadrants. *J. Magn. Res.* **48**, 286–292.
30. Plateau, P. & Guéron, M. (1982). Exchangeable proton NMR without base-line distortion, using new strong-pulse sequences. *J. Am. Chem. Soc.* **104**, 7310–7311.
31. Piotto, M., Saudek, V. & Sklenar, V. (1992). Gradient-tailored excitation for single-quantum NMR spectroscopy of aqueous solutions. V. *J. Biomol. NMR* **2**, 661–665.
32. Rance, M., Sørensen, O.W., Bodenhausen, G., Wagner, G., Ernst, R.R. & Wüthrich, K. (1983). Improved spectral resolution in cosy 1H NMR spectra of proteins via double quantum filtering. *Biochem. Biophys. Res. Commun.* **117**, 479–485.
33. Bax, A. & Davis, D.G. (1985). MLEV-17 based two-dimensional homonuclear magnetization transfer spectroscopy. *J. Magn. Res.* **65**, 355–366.
34. Jeener, J., Meier, B.H., Bachmann, P. & Ernst, R.R. (1979). Investigation of exchange processes by two dimensional NMR spectroscopy. *J. Chem. Phys.* **71**, 4546–4553.
35. Griesinger, C., Otting, G. & Wüthrich, K. (1988). Clean TOCSY for ^{1}H spin system identification in macromolecules. *J. Am. Chem. Soc.* **110**, 7870–7872.
36. Sklenar, V., Miyashiro, H., Zon, G., Miles, H.T. & Bax, A. (1986). Assignment of the ^{31}P and ^{1}H resonances in oligonucleotides by two dimensional spectroscopy. *FEBS Lett.* **208**, 94–98.
37. Brünger, A.T. (1992). *X-PLOR. A System for X-ray Crystallography and NMR*. Yale University Press, New Haven, CT.
38. Lavery, R. & Sklenar, H. (1988). The definition of generalized helicoidal parameters and of axis curvature for irregular nucleic acids. *J. Biomol. Struct. Dyn.* **6**, 63–91.
39. Lavery, R. & Sklenar, H. (1989). Defining the structure of irregular nucleic acids: conventions and principles. *J. Biomol. Struct. Dyn.* **6**, 655–667.
40. Esnouf, R.M. (1997). An extensively modified version of MolScript that includes greatly enhanced coloring capabilities. *J. Mol. Graph.* **15**, 132–134.
41. Kraulis, P.J. (1991). MOLSCRIPT a program to produce both detailed and schematic plots of protein structures. *J. Appl. Cryst.* **24**, 946–950.
42. Merritt, E.A. & Bacon, D.J. (1997). Raster3D: photorealistic molecular graphics. *Methods Enzymol.* **277**, 505–524.